

**Multilayer manifold and sparsity constrained nonnegative matrix factorization for hyperspectral unmixing**

Author

Shu, Zhenqiu, Zhou, Jun, Tong, Lei, Bai, Xiao, Zhao, Chunxia

Published

2015

Conference Title

2015 IEEE INTERNATIONAL CONFERENCE ON IMAGE PROCESSING (ICIP)

Version

Accepted Manuscript (AM)

DOI

[10.1109/ICIP.2015.7351186](https://doi.org/10.1109/ICIP.2015.7351186)

Rights statement

© 2015 IEEE. Personal use of this material is permitted. Permission from IEEE must be obtained for all other uses, in any current or future media, including reprinting/republishing this material for advertising or promotional purposes, creating new collective works, for resale or redistribution to servers or lists, or reuse of any copyrighted component of this work in other works.

Downloaded from

<http://hdl.handle.net/10072/169474>

Griffith Research Online

<https://research-repository.griffith.edu.au>

# MULTILAYER MANIFOLD AND SPARSITY CONSTRAINED NONNEGATIVE MATRIX FACTORIZATION FOR HYPERSPECTRAL UNMIXING

Zhenqiu Shu<sup>1</sup>, Jun Zhou<sup>2</sup>, Lei Tong<sup>2</sup>, Xiao Bai<sup>3</sup>, Chunxia Zhao<sup>1</sup>

<sup>1</sup>School of Computer Science and Engineering, Nanjing University of Science and Technology, Nanjing, Jiangsu, China

<sup>2</sup>Institute for Integrated and Intelligent Systems, Griffith University, Nathan, QLD, Australia

<sup>3</sup>School of Computer Science and Engineering, Beihang University, Beijing, China

## ABSTRACT

Given a hyperspectral image, unmixing tries to estimate the spectral responses of the latent constituent materials and their corresponding fractions. Recently, Nonnegative Matrix Factorization (NMF) has been widely applied to solve the hyperspectral unmixing problem because of its plausible physical interpretation. In this paper, we propose a novel method, Multilayer Manifold and Sparsity constrained Nonnegative Matrix Factorization (MMSNMF), for hyperspectral unmixing. In this approach, Multilayer NMF decomposes a hyperspectral image iteratively at several layers. In order to consider both the manifold structure of hyperspectral image and the sparsity of abundance matrix, we impose a graph regularization term and a sparsity regularization term on both the spectral signature matrix and the abundance matrix. Experimental results on both synthetic and real data validate the effectiveness of the proposed method in hyperspectral unmixing.

**Index Terms**— NMF, hyperspectral unmixing, sparsity, manifold structure, graph regularization

## 1. INTRODUCTION

Unmixing has played an important role in the preprocessing step of hyperspectral image analysis due to the limited spatial resolution of imaging sensors[1]. This technique has attracted more and more attention in both remote sensing and ground-based applications[2, 3]. The goal of hyperspectral unmixing is to decompose an image into a collection of spectral signatures, called *endmembers*, and their corresponding proportion, called *abundance*, at each spatial location.

Nonnegative Matrix Factorization (NMF)[4, 5] is a popular linear unmixing method to deal with the blind source separation (BSS) problem, which has been widely applied to hyperspectral unmixing. NMF-based hyperspectral unmixing

tries to estimate an endmember matrix and an abundance matrix, and uses their product to approximate to the original hyperspectral image. In order to make use of prior knowledge, various constraints have been imposed on NMF approaches to achieve different goals. Minimum volume constrained NMF (MVCNMF)[6] was proposed from a convex geometric point of view to drive the virtual endmembers to enclose the data cloud but with minimum volume. Wang *et al.*[7] employed endmembers dissimilarity as a constraint, which is used to measure the difference between endmember signatures and to force the signatures to be smooth. In order to take advantage of the sparsity of abundances in hyperspectral image, Qian *et al.*[8] proposed a sparsity constrained NMF (SNMF) unmixing method. In SNMF, each mixing pixel can be represented by a linear combination of only few endmembers by applying a  $L_{1/2}$  regularizer on the abundance matrix. Jia *et al.*[9] also imposed sparsity constraints on the NMF model, but further incorporated a piecewise smoothness term.

Alternatively, to consider the geometric data structure of hyperspectral images, Lu *et al.*[10] proposed a graph-regularized  $L_{1/2}$ -NMF (GLNMF) method for hyperspectral unmixing. GLNMF tries to impose the manifold regularization and sparseness constraints on the abundance matrix. Cichocki *et al.*[11] proposed a multilayer NMF (MNMF), in which multilayer structure is used to decompose the original data matrix. Rajabi *et al.*[12] further extended this approach by adding a sparsity constraint to both spectral and abundance matrix in each layer. However, one of the disadvantages in this approach is that it has neglected the geometric manifold structure of both spectral signatures and abundance fractions in each layer, which is an important property of the hyperspectral data.

In this paper, we propose a novel unmixing method, namely Multilayer Manifold and Sparsity constrained Nonnegative Matrix Factorization (MMSNMF), which takes full advantage of the latent manifold structure and sparseness of hyperspectral images, simultaneously. In each layer, we in-

This work was supported by the Grants of the National Natural Science Foundation of China [Gran No.61272220, 61401214].

corporate dual Laplacian graphs that capture manifold structures in both spectral and spatial domain, and an  $L_{1/2}$  sparsity constraint for spectral signatures as well as abundance fractions. Experimental results show that the proposed method can obtain promising performance in hyperspectral unmixing.

The rest of the paper is organized as follows. Section 2 introduces the background of hyperspectral unmixing based on NMF. Section 3 presents the MMSNMF approach. To verify the effectiveness of the proposed method, the experimental evaluations are presented in Section 4. Finally, conclusions are drawn in Section 5.

## 2. RELATED WORK

In this section, we introduce how to employ NMF to linearly unmix the hyperspectral image.

Suppose that a hyperspectral image  $X \in \mathbb{R}^{L \times I}$  contains  $c$  spectral signatures where  $x_i \in \mathbb{R}^{L \times 1}$  is an observed vector at  $i$ -th pixel with  $L$  spectral bands. NMF aims to find an endmember matrix  $A \in \mathbb{R}^{L \times N}$  and an abundance matrix  $M \in \mathbb{R}^{N \times I}$  to approximate the origin nonnegative matrix using a linear mixing model:

$$X = AM + E \quad (1)$$

where  $E \in \mathbb{R}^{L \times I}$  denotes the additive noise, and  $N$  is the number of endmembers. Thus, the objective function of NMF can be expressed as:

$$\begin{aligned} \min_{A, M} O(A, M) &= \frac{1}{2} \|X - AM\|_F^2 \\ \text{s.t. } &A \geq 0, M \geq 0 \end{aligned} \quad (2)$$

where  $\|\cdot\|_F$  denotes the Frobenius norm. NMF has been easily extended by adding different constraints, such as MVC-NMF, SNMF, GLNMF and DGNMF[13]. Similarly, our method is also based on the standard NMF.

## 3. THE PROPOSED METHOD

In this section, we first describe the structure of Multilayer NMF[11, 12]. Then the objective function of the proposed method and the corresponding iterative updating rules are described.

### 3.1. The Multilayer Structure

In multilayer structure, the optimization sub-problem in each layer can provide more accurate estimation than the initial estimation of endmembers and abundance matrices by VCA. It can also avoid getting stuck in local minima during optimization process[11]. In the first layer, the original data matrix is decomposed into matrices  $A_1$  and  $M_1$ . Then the result of the first layer ( $M_1$ ) is used as the input data for the second layer, which is further decomposed into  $A_2$  and  $M_2$ . This decomposition process is repeated to reach the maximum number of

layers ( $P$ ). Fig.1 shows the structure of the multilayer NMF. Meanwhile, we can give the mathematical definition of multilayer NMF as follows:

$$X = A_1 M_1, M_1 = A_2 M_2, \dots, M_{P-1} = A_P M_P \quad (3)$$

Thus, the endmember signature matrix and the abundances matrix can be written as follows:

$$\begin{cases} A = A_1 A_2 \dots A_P \\ M = M_P \end{cases} \quad (4)$$

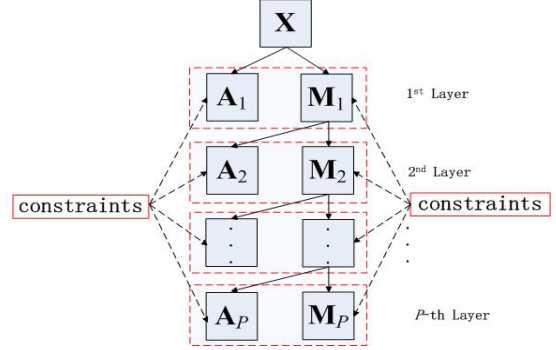


Fig. 1 The structure of multilayer NMF

### 3.2. MMSNMF

Previous studies[14, 15] have shown that not only data points, but also features are sampled from some low-dimensional manifolds in many pattern recognition tasks. Meanwhile, it has been pointed out that hyperspectral data lies on a low-dimensional submanifold embedded in the high-dimensional ambient space[10]. Thus, not only the abundances lie on a nonlinear low dimensional manifold, namely abundance manifold, but also the endmembers lie on a nonlinear manifold, namely endmember manifold. Therefore, we employ two graphs, i.e., abundance graph and endmember graph to characterize the geometric structures of the two manifolds, respectively.

Given a data set  $X = [x_1, \dots, x_I] \in \mathbb{R}^{L \times I}$ , an abundance graph  $G^A = \{X, W^A\}$  can be constructed with data set  $X$ , where  $W^A$  denotes a weighted matrix. The elements of the matrix  $W^A$  can be defined as:

$$W_{ij}^A = \begin{cases} 1 & \text{if } x_i \in N_p(x_j) \text{ or } x_j \in N_p(x_i) \\ 0 & \text{otherwise} \end{cases} \quad (5)$$

where  $N_p(x_j)$  is the set of  $p$  nearest neighbors of  $x_j$ ,  $L^A = D^A - W^A$  is the Laplacian matrix,  $D^A$  is a diagonal matrix and  $D_{ii}^A = \sum_j W_{ij}^A$ .

Meanwhile, we also need to construct an endmember graph  $G^M = \{X^T, W^M\}$  whose vertices correspond to  $X^T = [x_1^T, \dots, x_L^T] \in \mathbb{R}^{I \times L}$ . Thus, the elements of the weighted matrix  $W^M$  can be defined as:

$$W_{ij}^M = \begin{cases} 1 & \text{if } x_i^T \in N_p(x_j^T) \text{ or } x_j^T \in N_p(x_i^T) \\ 0 & \text{otherwise} \end{cases} \quad (6)$$

where  $L^M = D^M - W^M$  is the Laplacian matrix,  $D^M$  denotes a diagonal matrix and  $D_{ii}^M = \sum_j W_{ij}^M$ .

To take the manifold structure of the abundance fractions and the spectral signature into account, the dual graph regularization and  $L_{1/2}$  regularizer are incorporated into multi-layer NMF. As a result, the objective function of MMSNMF for the  $l$ -th layer can be represented as follows:

$$O_l = \frac{1}{2} \|X_l - A_l M_l\|_F^2 + \lambda_A \|A_l\|_{1/2} + \lambda_M \|M_l\|_{1/2} + \frac{\beta_A}{2} \text{Tr}(A^T L_l^A A) + \frac{\beta_M}{2} \text{Tr}(M^T L_l^M M) \quad (7)$$

where  $\lambda_A$  and  $\lambda_M$  denote the regularization parameters to balance the sparsity of the spectral signature and the abundance fractions.  $\beta_A$  and  $\beta_M$  are the dual graph regularization parameters. In this model, the first term is used to measure the reconstruction error. The second and third terms are designed to force the sparseness of the endmember matrix and the abundance matrix. The last two terms are used to explore both the abundance manifold and the endmember manifold of hyperspectral images.

Let  $(\psi_{ik})_l$  and  $(\varphi_{jk})_l$  be the Lagrange multipliers for constraints  $(A_{ik})_l \geq 0$  and  $(M_{jk})_l \geq 0$ , respectively. We take the partial derivatives of Lagrange  $\mathcal{L}_l$  over  $A_l$  and  $M_l$  of Eq. (7) as follows:

$$\frac{\partial \mathcal{L}_l}{\partial A_l} = -X_l M_l^T + A_l M_l^T M_l + \frac{\lambda_A}{2} A_l^{-\frac{1}{2}} + \beta_A L_l^A A_l + \Psi \quad (8)$$

$$\frac{\partial \mathcal{L}_l}{\partial M_l} = -A_l^T X_l + A_l^T A_l M_l + \frac{\lambda_M}{2} M_l^{-\frac{1}{2}} + \beta_M L_l^M M_l + \Phi \quad (9)$$

Using Karush-Kuhn-Tucker conditions  $(\psi_{ik} A_{ik})_l = 0$  and  $(\varphi_{jk} M_{jk})_l = 0$ , we can obtain:

$$(-X_l M_l^T + A_l M_l^T M_l + \frac{\lambda_A}{2} A_l^{-\frac{1}{2}} + \beta_A L_l^A A_l) \cdot A_l = 0 \quad (10)$$

$$(-A_l^T X_l + A_l^T A_l M_l + \frac{\lambda_M}{2} M_l^{-\frac{1}{2}} + \beta_M L_l^M M_l) \cdot M_l = 0 \quad (11)$$

From Eq. (10) and Eq. (11), the following update rules can be derived:

$$A_l \leftarrow A_l \cdot \frac{X_l M_l^T + \beta_A A_l W_l^A}{A_l M_l^T M_l + \frac{\lambda_A}{2} A_l^{-\frac{1}{2}} + \beta_A A_l D_l^A} \quad (12)$$

$$M_l \leftarrow M_l \cdot \frac{A_l^T X_l + \beta_M M_l W_l^M}{A_l^T A_l M_l + \frac{\lambda_M}{2} M_l^{-\frac{1}{2}} + \beta_M M_l D_l^M} \quad (13)$$

## 4. EXPERIMENTS

In this section, we carry out some experiments to verify the effectiveness of the proposed method in hyperspectral unmixing. The proposed method is compared with VCA[16], NMF,  $L_{1/2}$ -NMF[8] and Multilayer NMF (MNMF)[12]. The Spectral Angle Distance (SAD) and Abundance Angle Distance

(AAD) are used to evaluate the performance of the unmixing methods. Their detailed definitions can be found in[12].

### 4.1. Synthetic Data

We first evaluated the proposed method on a synthetic data. To generate the synthetic data, we randomly selected six spectral signatures from the USGS digital spectral library[17]. This synthetic data are generated by the following steps. First, we generate a  $64 \times 64$  image and then divide it into  $8 \times 8$  blocks. Second, each block is filled up by only one type of signature randomly chosen from the candidate signatures, and then a low pass filter of size  $9 \times 9$  is applied to generate the mixed data. For pixels with abundances larger than 80%, the abundances are replaced with a mixture of all endmembers with equally distributed abundances.

To evaluate the robustness of the proposed method in the presence of noise, a zero-mean Gaussian noise is added to the synthetic data. The signal-to-noise ratio (SNR) can be defined as:

$$SNR = 10 \log_{10} \frac{E[x^T x]}{E[e^T e]}$$

where  $x$  and  $e$  represent the observation and noise of a pixel, respectively and  $E[\cdot]$  denotes the expectation operator.

In the first experiment, we evaluate the performances of all methods in hyperspectral unmixing under the same noise. Here, the signal-to-noise ratio (SNR) is set to 20. Similar to MNMF, the sparseness regularization parameter  $\lambda_A$  of the proposed method is set as:

$$\lambda_A = \lambda_0 e^{-\frac{t}{\tau}}$$

where  $t$  denotes the number of iterations and  $\tau$  is a constant parameter. In this experiment, we set the parameters as follows:  $\lambda_0=0.1$ ,  $\tau=25$ ,  $P=10$ ,  $T_{\max}=300$ ,  $\lambda_M = 2\lambda_A$  and  $\beta_A = \beta_M = 0.5$ . The experimental process is repeated 10 times and then the average performance is taken as the final result. Fig. 2 shows the unmixing results in terms of mean and standard deviation of the criteria. It can be seen that the proposed method has achieved the best performance among all methods.

In the second experiment, we evaluate the performance of the proposed method under different noise. Table 1 shows the results of all methods under different SNR. It can be found that the root mean square errors of both SAD and AAD of the proposed method are superior to those from the other methods no matter how the SNR changes.

### 4.2. Real Remote Sensing Data

The third experiment is carried out on the Jasper Ridge dataset[18]. We conduct the unmixing experiment on a subimage with  $100 \times 100$  pixels whose ground truth is given[19]. The first pixel corresponds to the pixel (105, 269) in the original image. After we remove some water absorption bands,

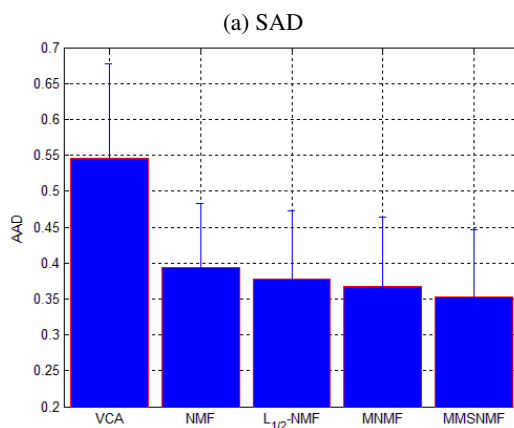
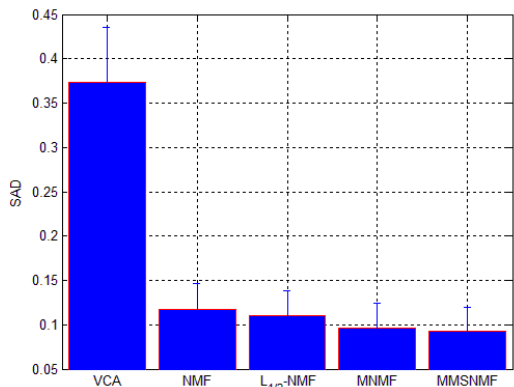


Fig. 2 Performances of different methods

such as 1–3, 108–112, 154–166 and 220–224, 198 bands are left in the subimage. In total, 4 types of endmembers including road, soil, water and tree are used.

In this experiment, the setting of the parameters is the same as the previous experiments. Fig. 3 shows the results of abundance estimation on the Jasper Ridge data. From the 1<sup>st</sup> to the 4<sup>th</sup> column, they are the abundances of road, water, tree and soil. The first row displays the ground truth for the abundance fractions of the endmembers, and the second row shows the abundance maps of endmembers estimated by our method. Both figures are in grayscale, in which a dark pixel indicates that the abundance of the relative endmember is low, and vice versa. Table 2 shows the root mean square errors of SAD of the endmember estimation with all the unmixing methods. The results demonstrate that the average performance of the proposed method is better than other comparison methods. The main reason is that our proposed method not only takes into account the sparsity of hyperspectral image, but also discovers the manifold structure of the spectral signatures and the abundance fractions in each layer.

## 5. CONCLUSION

In this paper, a novel method, called multilayer manifold and sparsity constrained nonnegative matrix factorization, is proposed to take advantage of intrinsic manifold structure

Table 1 The result of different SNR

(a) SAD					
SNR	VCA	NMF	$L_{1/2}$ -NMF	MNMF	MMSNMF
15	0.4481	0.1111	0.1038	0.0917	<b>0.0903</b>
20	0.4295	0.0715	0.0662	0.0698	<b>0.0647</b>
25	0.468	0.0882	0.0832	0.0809	<b>0.0773</b>
30	0.3916	0.0926	0.0900	0.0814	<b>0.0797</b>
35	0.5049	0.0744	0.0716	0.0635	<b>0.0613</b>
40	0.5129	0.0443	0.0430	0.0429	<b>0.0396</b>
Avg	0.4592	0.0804	0.0763	0.0717	<b>0.0688</b>

(b) AAD					
SNR	VCA	NMF	$L_{1/2}$ -NMF	MNMF	MMSNMF
15	0.5576	0.3640	0.3665	0.3656	<b>0.3618</b>
20	0.4695	0.3263	0.3256	0.3272	<b>0.3246</b>
25	0.5078	0.3468	0.3461	0.3444	<b>0.3432</b>
30	0.3211	0.1920	0.1919	0.1909	<b>0.1903</b>
35	0.3477	0.1822	0.1819	0.1811	<b>0.1803</b>
40	0.4032	0.2465	0.2325	0.2332	<b>0.2314</b>
Avg	0.4345	0.2763	0.2741	0.2737	<b>0.2719</b>

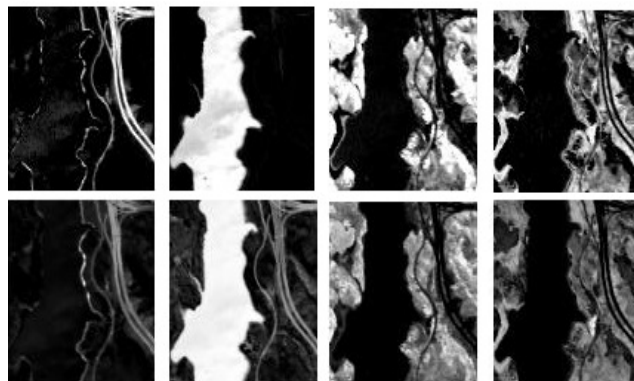


Fig.3 Abundance maps of different endmembers

of the hyperspectral images. In each layer, the proposed method enforces both manifold and sparsity constraints on the spectral signatures and abundance fractions. Compared with other state-of-the-art methods, the superiority of the proposed method in hyperspectral unmixing has been validated on both synthetic and real data.

## References

- [1] N. Keshava, "A survey of spectral unmixing algorithms," *Lincoln Laboratory Journal*, vol. 14, no. 1, pp. 55–78, 2003.
- [2] J. Bioucas-Dias, A. Plaza, and N. Dobigeon, "Hyperspectral unmixing overview: Geometrical, statistical, and sparse regression-based approaches," *IEEE Journal of Selected Topics in Applied Earth Observations and Remote Sensing*, vol. 5, no. 2, pp. 354–379, 2012.
- [3] A. Goetz, G. Vane, and Solomon J., "Imaging spectrometry for earth remote sensing," *Science*, vol. 228, no. 4704, pp. 1147–1153, 1985.
- [4] D. D. Lee and H. S. Seung, "Learning the parts of objects by

Table 2 Comparison between methods in terms of SAD

Endmember	VCA	NMF	$L_{1/2}$ -NMF	MNMF	MMSNMF
Road	0.2588	0.1920	0.1941	0.1746	<b>0.1734</b>
Water	<b>0.0330</b>	0.0906	0.0827	0.0494	0.0481
Tree	0.1325	0.1534	0.1508	0.1324	<b>0.1311</b>
Soil	0.1176	0.1177	0.1130	0.0870	<b>0.0857</b>
Avg	0.1355	0.1384	0.1352	0.1190	<b>0.1096</b>

WhitepapersDetail, 2013, Online.

- [19] F. Zhu, Y. Wang, S. Xiang, B. Fan, and C. Pan, "Structured sparse method for hyperspectral unmixing," *ISPRS Journal of Photogrammetry and Remote Sensing*, vol. 88, pp. 101–118, 2014.
- non-negative matrix factorization," *Nature*, vol. 401, no. 6755, pp. 788–791, 1999.
- [5] D. D. Lee and H. S. Seung, "Algorithms for non-negative matrix factorization," *Advances in Neural Information Processing Systems* 13, 2001, pp. 556–562, MIT Press.
- [6] L. Miao and H. Qi, "Endmember extraction from highly mixed data using minimum volume constrained nonnegative matrix factorization," *IEEE Transactions on Geoscience and Remote Sensing*, vol. 45, no. 3, pp. 765–777, 2007.
- [7] N. Wang, B. Du, and L. Zhang, "An endmember dissimilarity constrained non-negative matrix factorization method for hyperspectral unmixing," *IEEE Journal of Selected Topics in Applied Earth Observations and Remote Sensing*, vol. 6, no. 2, pp. 554–569, 2013.
- [8] Y. Qian, S. Jia, J. Zhou, and et al., "Hyperspectral unmixing via  $L_{1/2}$  sparsity-constrained nonnegative matrix factorization," *IEEE Transactions on Geoscience and Remote Sensing*, vol. 49, no. 11, pp. 4282–4297, 2011.
- [9] S. Jia and Y. Qian, "Constrained nonnegative matrix factorization for hyperspectral unmixing," *IEEE Transactions on Geoscience and Remote Sensing*, vol. 47, no. 1, pp. 161–173, 2009.
- [10] X. Lu, H. Wu, Y. Yuan, P. Yan, and X. Li, "Manifold regularized sparse NMF for hyperspectral unmixing," *IEEE Transactions on Geoscience and Remote Sensing*, vol. 51, no. 5, pp. 2815–2826, 2013.
- [11] A. Cichocki and Z. Rafal, "Multilayer nonnegative matrix factorisation," *Electronics Letters*, vol. 42, no. 16, pp. 947–968, 2006.
- [12] R. Rajabi and H. Ghassemian, "Spectral unmixing of hyperspectral imagery using multilayer NMF," *IEEE Geoscience and Remote Sensing Letters*, vol. 12, no. 1, pp. 38–42, 2015.
- [13] L. Tong, J. Zhou, X. Bai, and Y. Gao, "Dual graph regularized NMF for hyperspectral unmixing," *Proc. in DICTA*, 2014.
- [14] M. Belkin and P. Niyogi, "Laplacian eigenmaps and spectral techniques for embedding and clustering," *Advance Neural Informaion Processing System (NIPS)*, vol. 14, 2001.
- [15] F. Shang, L. Jiao, and F. Wang, "Graph dual regularization non-negative matrix factorization for co-clustering," *Pattern Recognition*, vol. 45, no. 6, pp. 2237–2250, 2012.
- [16] J. Nascimento and J. Dias, "Vertex component analysis: A fast algorithm to unmix hyperspectral data," *IEEE Transactions on Geoscience and Remote Sensing*, vol. 43, no. 4, pp. 898–910, 2005.
- [17] R. Clark, G. Swayze, R. Wise, E. Livo, T. Hoefen, R. Kokaly, and S. Sutley, "USGS Digital Spectral Library Splib06a:U.S. Geological Survey, Digital Data Series 231," <http://speclab.cr.usgs.gov/spectral.lib06>, 2007, Online.
- [18] Envi-Tutorials, "Envi classic vegetation hyperspectral analysis," <http://www.exelisvis.com/Learn/>